Struct Chem (2016) 27:1303–1315
DOI 10.1007/s11224-016-0781-2

ORIGINAL RESEARCH

Structural similarities and diversity in a series of crystalline solids composed of 2-aminopyridines and glutaric acid

Sergiu Draguta[1] · Marina S. Fonari[1,2] · Shabari Nath Bejagam[1] · Kathryn Storms[1] · Jennifer Lindline[1] · Tatiana V. Timofeeva[1]

Received: 22 April 2016 / Accepted: 24 May 2016 / Published online: 2 June 2016

Abstract A solvent co-crystallization of three 2-aminopyridine derivatives, 2-aminopyridine (AP), 2-amino-6-methylpyridine (AMP), and 2,6-diaminopyridine (DAP) with the odd-membered propane-1,3-dicarboxylic acid ($C_5H_{12}O_4$ = GAH_2, glutaric acid) resulted in six ionic crystalline products, (HAP)(GAH) (**1**), (HAMP)(GAH) (**2**, **3**), (HDAP)(GAH) (**4**), $(HDAP)_2(GA)$ (**5**), and $(HDAP)_2$ (DAP)(GA)(EtOH) (**6**, EtOH = ethanol). New compounds were characterized by single-crystal and powder X-ray diffraction, melting points, and IR spectra. The proton transfer to the pyridine nitrogen atom in all compounds and the location of H-atom in the carboxylic group in the hydrogen glutarate anion in binary adducts **1**–**4** was determined reliably from the low-temperature X-ray experiments. All compounds adopt the recurring $R_2^2(8)$ 2-aminopyridine–carboxylic acid heteromeric supramolecular synthon. The aggregation of hydrogen glutarate anions in the C(8) chain motifs in **1**–**4** occurs via the homomeric $COOH\cdots COO^-$ robust pattern. Adducts **2** and **3** represent conformational polymorphs; adducts **4**, **5** and **6** reveal the diversity in the components' forms (ionic and neutral), acid–base ratios (1:1, 1:2, and 1:3), and hydrogen-bonding systems. This work demonstrates the variety of forms of glutaric acid in the H-bonded adducts.

Keywords Glutaric acid · 2-Aminopyridine · Crystal engineering · Hydrogen bonds

Introduction

Over the past few decades dicarboxylic acids especially those updated by the generally regarded as safe (GRAS) list of the US Food & Drug Administration (FDA) proved their special place in the crystal engineering among the co-crystal formers to improve the absorption, distribution, metabolism, elimination, and toxicity (ADMET) characteristics of existing drugs with the perspective for multi-component compounds which they comprise to be considered by pharmaceutical industry as better-quality medicines [1–7]. Otherwise, the relevance of dicarboxylic acids and dicarboxylate anions in biological and industrial processes required that such species would be easily detected and quantified [8, 9]. The elaboration of synthetic receptors, where the heterocyclic units attached to the rigid and semirigid Troger's base molecular frameworks, could potentially serve for hydrogen bonding being sensitive to the recognition of dicarboxylate anions and dicarboxylic acids, launched in the 1990s of the last century [10–12]. Since then the 2-aminopyridine moiety, giving a robust and reoccurring hydrogen-bonding motif when being coupled with the carboxylic acid group, appeared as a common co-former for the formation of hydrogen-bonded complexes with dicarboxylic acids. Along with the 2-aminopyridine–carboxylic acid heterosynthon of repetitive occurrence, the robust pyridine–carboxylic acid heterosynthon attested its efficacy in crystal engineering [13–16] since a lot of drugs contain in their molecular scaffolds these fragments favorable for H bonding. The homologous series of even- and odd-membered carboxylic acids reveal some

Electronic supplementary material The online version of this article (doi:10.1007/s11224-016-0781-2) contains supplementary material, which is available to authorized users.

✉ Tatiana V. Timofeeva
tvtimofeeva@nmhu.edu

[1] Department of Biology and Chemistry, New Mexico Highlands University, Las Vegas, NM 87701, USA

[2] Institute of Applied Physics ASM, Chişinău, Republic of Moldova

distinctive features in co-crystallization experiments with drugs and biologically relevant molecules explained by the difference in their physical characteristics (melting point, volumetric thermal expansion) and inherent symmetry [17, 18].

In our recent study, we have shown the reoccurrence of the robust pyridine–carboxylate and 2-aminopyridine–carboxylate heterosynthons in twelve organic solids produced by combination of five aminopyridines with three even-membered dicarboxylic acids, succinic acid, sebacic acid, $(HOOC)_2(CH_2)_n$, $n = 2$, 8; and fumaric acid, $(HOOC)_2(CH)_n$, $n = 2$ [19]. In continuation of that research, this contribution presents six adducts of three 2-aminopyridines with the odd-membered glutaric acid, $(HOOC)_2(CH_2)_n$, $n = 3$ (Scheme 1).

In addition to being a natural component of dietary products, glutaric acid is a normal metabolic intermediate of fatty acid, tryptophan, and lysine metabolism [3]. Although one of the M. Etter's pioneering works dated back to 1995 has demonstrated the perfect H-bonded fit between glutaric acid and urea in the 1:2 adduct [20], later on it was declared that the formation of multimolecular compounds between the C3 or C5 dicarboxylic acids and drug molecules (itraconazole = ITZ in particular) has been considered as unachievable [2]. The authors hypothesized that co-crystals could not be made since the geometric fit was considered to be more important than acid–base chemistry in directing crystallization with the odd-membered dicarboxylic acids, and the H-bonded trimers with the odd-chain dicarboxylic acids require a significant departure from their minimal energy conformation, as the latter is characterized by an angle of approximately 120° between the two OH^- groups [21, 22]. Nevertheless, in 2013, another group of researchers succeeded in obtaining the 1:1 co-crystals of ITZ with the malonic (C3), glutaric (C5), and pimelic (C7) acids, which all have an odd number of carbon atoms in their chains [23]. So far, by survey the available open literature sources and the Cambridge Structural Database, we identified a series of adducts of glutaric acid with drugs and biologically relevant molecules in the form of *co-crystals* with N-(2-pyridyl)acetamide), isonicotinamide, N-(pyridin-2-yl)isonicotinamide, meloxicam, caffeine, isonicotinohydrazide, nevirapine, sulfathiazole, carbamazepine, nicotinamide, acyclovir, praziquantel, nitazoxanide, fluconazole, theophylline [13, 14, 21, 24–35], and *salts* with trimethoprim, lamotrigine, trospium chloride, pyrimethamine, sildenafil, and tetracycline [36–41]. The inspection of these data reveals the structural and polymorphic diversities [14, 23, 42, 43] of the final multicomponent forms dictated by the possibility of neutral/ionic forms of the components (neutral molecule, mono-, di-deprotonated anion in the case of GAH_2), and confirmation flexibility of glutaric acid/glutarate anion in these adducts.

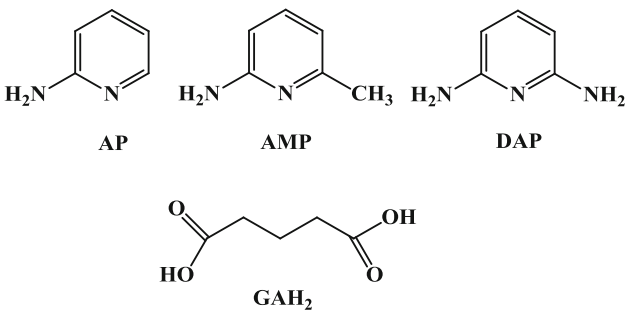

Scheme 1 Schematic presentation of base and acid molecules used in this study

Since the structure of 2-aminopyridine sustains an ideal geometry for the assembly with the carboxylic acid group, herein we report the results of co-crystallization of three 2-amino-substituted pyridine derivatives, 2-aminopyridine itself (AP), 2-amino-6-methylpyridine (AMP), and 2,6-diaminopyridine (DAP) with the odd-membered propane-1,3-dicarboxylic (glutaric) acid ($C_5H_{12}O_4 = GAH_2$) (Scheme 1) that is resulted in six ionic crystalline adducts, (HAP)(GAH) **1**; (HAMP)(GAH) **2**, **3**; (HDAP)(GAH) **4**; $(HDAP)_2(GA)$ **5**; and $(HDAP)_2(DAP)(GA)(EtOH)$ **6**, where EtOH = ethanol (Scheme 2).

The products are characterized by the Fourier transform infrared (FT-IR) spectra, melting points, single-crystal and powder diffraction X-ray data. The structural aspects including the conformation of the molecules and the hydrogen-bonding patterns are discussed. Though the X-ray data for adduct **4** have been reported recently [44], we include our own results for this adduct in this contribution since we report the low temperature data (RT data in [44]) and monitor the structural similarities between **3** and **4**. The structural diversities in the system DAP–GAH_2 (adducts **4**, **5**, and **6**) are also reported and discussed.

Experimental

Materials and physical measurements

All chemicals were purchased from Aldrich and used without further purification. Melting points were determined on a Stanford Research System (SRS) melting point apparatus and are uncorrected. IR spectra were registered using ATR accessory at Nicolet Magna-IR 550 having Omnic software version 7.3 equipped with Spectra-Tech foundation series ZnSe and ORIGIN JASCO spectrometers. The powder diffraction data were collected with a SIETRONICS XRD SCAN X-ray powder diffractometer equipped with a Cu-Kα radiation (λ = 1.54056 Å) source.

Scheme 2 Schematic presentation of crystalline adducts obtained in this study

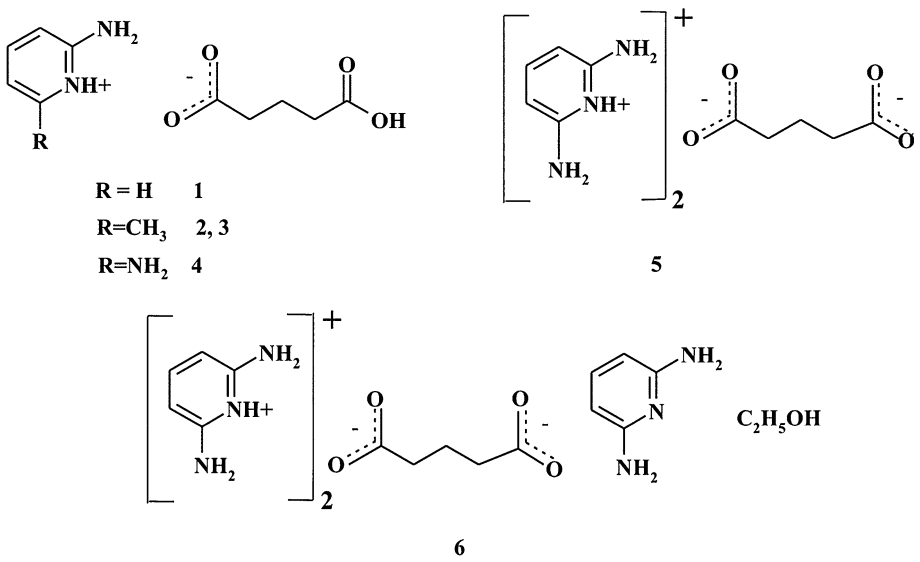

The diffractometer was operated at 30 kV and 35 mA. The data were collected over an angle range of 5°–40° 2θ at a scanning speed of 5° 2θ per minute.

Co-crystallization experiments

The slow evaporation method was used to co-crystalize the pyridine bases with GAH_2 using methanol or ethanol solvents. The spectroscopic grade solvents employed for the crystallization purpose were of the highest available purity. All molecular adducts were prepared similarly by dissolving separately GAH_2 and the corresponding amine listed in Scheme 1 in a suitable solvent (either CH_3OH or C_2H_5OH), mixing these solutions, and then by slow evaporation the obtained solution. Single crystals were obtained in a few days in all the cases. In a typical example, 13.2 mg (0.1 mmol) of GAH_2 and 9.4 mg (0.1 mmol) of AP were dissolved in separate tubes in 5 mL of CH_3OH each, then mixed and allowed for slow evaporation at ambient conditions. Good-quality single crystals **1** suitable for X-ray diffraction study were obtained in 48 h.

(HAP)(GAH) (**1**), M.P. 102–104 °C, IR (cm^{-1}): 3735w, 2360s, 2343s(sh), 1700w, 1653w, 1558w, 1507w.
(HAMP)(GAH) (**2**), M.P. 134–136 °C, IR (cm^{-1}): 3309w, 3033w, 2360s, 1750m, 1665s, 1605m, 1550m, 1406s, 1350m, 1308s, 1250m, 1200s, 1050m, 1000m, 950m, 802m, 758s.
$(HDAP)_2(GA)$ (**5**), M.P. 155 °C, IR: 3400w, 3000m, 2380w, 1900w, 1680s, 1550m, 1410s, 1330m, 1280m, 1180m, 960m, 850w, 750m, 700s, 645w, 625w.

X-ray crystallography

Single-crystal X-ray diffraction experiments were performed on a Bruker AXS SMART APEX CCD diffractometer equipped with a cryostat system [graphite monochromatic Mo Kα radiation, $\lambda = 0.71073$ Å] at 100 K for **1–5** and at a room temperature for **6**. Data integration and final unit cell parameters were obtained using SAINT + [45]. Absorption corrections were applied by a semiempirical approach using SADABS [46], and the crystal structures were solved by direct methods and refined using SHELXS and SHELXL program packages [47]. All non-H-atom positions were located using difference Fourier methods. In **3**, the carbonyl oxygen atom in the carboxylic group is disordered over two positions with the partial occupancies 0.528(7) and 0.472(7). The positions of H-atoms in the NH- and OH-groups were located from the difference Fourier maps and refined freely. The details of structures solution and refinement are given in Table 1, and the full geometric parameters are gathered in cif files.

Results and discussion

Synthesis and general properties

Co-crystallization from methanol solutions resulted in 1:1 adducts **1–4** in spite of whether 1:1 or 1:2 acid:base starting molar ratios have been used. When ethanol was used as a solvent, we have also obtained 1:1 adducts **1** and **2**, but from the 1:2 mixture, the adduct **5** with the stoichiometry 1:2 was obtained only for DAP, and the adduct **6** with quite unusual 1:3 acid:base ratio was obtained serendipitously,

Table 1 Crystal data and structure refinement details

	1	**2**	**3**	**4**	**5**	**6**
Empirical formula	$C_{10}H_{14}N_2O_4$	$C_{11}H_{16}N_2O_4$	$C_{11}H_{16}N_2O_4$	$C_{10}H_{15}N_3O_4$	$C_{15}H_{22}N_6O_4$	$C_{22}H_{35}N_9O_5$
Formula weight	226.23	240.26	240.26	241.25	350.39	505.59
Temperature (K)	100(2)	100(2)	100(2)	100(2)	100(2)	293(2)
Crystal system	Monoclinic	Orthorhombic	Orthorhombic	Orthorhombic	Monoclinic	Monoclinic
Space group	$P2_1/c$	$P2_12_12_1$	$P2_12_12_1$	$P2_12_12_1$	$P2_1/c$	$C2/c$
Z	4	4	4	4	4	8
a (Å)	5.1799(8)	4.9814(5)	4.8643(8)	5.1386(6)	7.980(3)	38.291(6)
b (Å)	22.227(3)	9.7872(9)	14.431(2)	14.9799(18)	7.181(3)	8.0933(13)
c (Å)	9.3131(14)	23.508(2)	17.009(3)	14.9894(18)	29.855(12)	19.425(3)
α (°)	90	90	90	90	90	90
β (°)	95.888(3)	90	90	90	94.918(7)	119.400(3)
γ (°)	90	90	90	90	90	90
V (Å^3)	1066.6(3)	1146.12(19)	1193.9(3)	1153.8(2)	1704.6(12)	5244.5(14)
d_{calcd} (g/cm^{-3})	1.409	1.392	1.337	1.389	1.365	1.281
μ (mm^{-1})	0.110	0.107	0.102	0.109	0.102	0.094
F(000)	480	512	512	512	744	2160
Reflections collected/unique	14,382/3279 [R(int) = 0.0423]	9336/2242 [R(int) = 0.0340]	13,137/2749 [R(int) = 0.0468]	31,788/3571 [R(int) = 0.0300]	3346 [R(int) = 0.0433]	22,864/4752 [R(int) = 0.0842]
Reflections with $[I > 2\sigma(I)]$	2593	2218	2389	3411	2711	2392
Data/restraints/parameters	3279/0/161	2242/0/172	3749/0/181	3571/0/178	3346/0/266	4752/21/371
Goodness of fit on F^2	1.025	1.024	1.051	1.047	1.025	0.913
R_1, wR_2 $[I > 2\sigma(I)]$	0.0436, 0.1107	0.0268, 0.0732	0.0392, 0.0901	0.0324, 0.0850	0.0412, 0.0937	0.0503, 0.1052
R_1, wR_2 (all data)	0.0577, 0.1171	0.0271, 0.0734	0.0487, 0.0949	0.0348, 0.0878	0.0553, 0.0985	0.1230, 0.1264
Largest diff. peak and hole (e Å^{-3})	0.413 and −0.247	0.149 and −0.216	0.322 and −0.247	0.308 and −0.177	0.170 and −0.222	0.220 and −0.194

whose synthesis we were not able to reproduce (Scheme 2). Of two polymorphs **2** and **3**, the latter also appeared as an elusive one which we were not able to reproduce in the consecutive attempts. The views of the crystals **1**, **2**, and **4** are displayed in Fig. 1. Powder X-ray diffraction studies have been used to check the samples purity. The experimental PXRD of **1**, **2**, and **5** is quite the same as those calculated using the single-crystal results (Fig. 1S in Supporting Information).

The results of melting point (MP) analysis for **1**, **2**, **4**, and **5** are shown as histograms in Fig. 2. Adducts have higher melting points than the pure GAH_2 most probably because of strong hydrogen bonds and an efficient close packing as it has been stated for co-crystals of isonicotinamide with alkanedicarboxylic acids [14].

Comparison of the solid-state IR spectra for **1**, **2**, **4**, **5** and starting components confirms the formation of new solid forms (Figs. 2S-4S). The IR spectra of the products display bands characteristic for intermolecular hydrogen bonding and stretching vibrations of N–H and O–H bonds in the interval 3735–3033 cm^{-1}, asymmetric and symmetric stretching vibrations of deprotonated carboxylic group at 1665 and 1406 cm^{-1}. The identification of C=N vibration represents rather difficult task since mixing of several bands in this region; the C–N stretching vibrations of aromatic amines were indicated by the bands in the region 1350–1200 cm^{-1}.The peaks in the range 1000–757 cm^{-1} were assigned to the 1,6-disubstituted pyridine ring, respectively.

X-ray study. Adducts with the 1:1 acid:base molar ratio

Four binary adducts of GAH_2 with three 2-aminopyridines (Scheme 1) with the compositions (HAP)(GAH) (**1**), (HAMP)(GAH) (**2**, **3**), and (HDAP)(GAH) (**4**) crystallize from methanol solution as colorless crystals with 1:1 acid:base molar ratio. Figure 3 depicts the views of formular units in **1–4**. The low-temperature single-crystal X-ray study reveals that all compounds represent organic salts with the proton transfer from one carboxylic group of GAH_2 to the pyridine nitrogen atom, resulting in formation of tight ionic pairs sustained by the same robust heteromeric $R_2^2(8)$ supramolecular synthon [48–51] typical for adducts of *ortho*-substituted aminopyridines with carboxylic acids [11, 13, 19, 46]; the donor–acceptor N···O distances being in the range 2.6797(13)–2.8453(15) Å, and NH···O angles being in the range 172(2)°–177(2)° (Table 2). The proton transfer to the pyridine nitrogen atom is also diagnosed by slight increase in the C–N–C bond angles in the base molecules [52] compared to that in non-protonated structures [53, 54], and the roughly equalized C–O distances in the deprotonated carboxylic group (Table 1S). Another carboxylic moiety remains intact without undergoing deprotonation like in other previously reported binary 1:1 adducts with GAH_2 [36, 55–58]. The backbone conformation of the hydrogen glutarate anion can be described by the two torsion angles, C(1)–C(2)–C(3)–C(4) and C(2)–C(3)–C(4)–C(5). As it is evident from the torsion angles listed in Table 1S, the GAH anion has *trans,trans*-conformation in **1** and **2** that affords the collinearity of carboxylic groups [14, 27], while it is in the *trans,gauche*-twisted conformation in **3** and **4** that affords the close to the perpendicular arrangement of these groups in **3**, with the dihedral angle between the COO^-/COOH moieties being 84.3(2)°, and almost antiparallel their arrangement in **4** where the same angle is equal to 19.2(3)°.

Compound **1** reveals significantly different crystal packing compared with **2–4**. First, adduct **1** packs in the monoclinic centrosymmetric $P2_1/c$ space group, while three other adducts **2–4** pack in the non-centrosymmetric orthorhombic $P2_12_12_1$ space group. The virtually planar binary adducts **1** are associated into centrosymmetric tetramer via $R_4^2(8)$ hydrogen-bonding pattern that is locked between the two above-mentioned $R_2^2(8)$ patterns, the planarity of tetramer being further supported by the two identical CH···O hydrogen bonds, C(7)–H(7)···O(2)($1 - x$, $2 - y$, $2 - z$), C···O = 3.2234(15) Å (Fig. 4a; Table 2). The aggregation of tetramers related by the glide plane *c* into the H-bonded layer occurs via COOH···COO^- hydrogen bond between two different carboxylic residues that combines the hydrogen glutarate anions in the C(8)

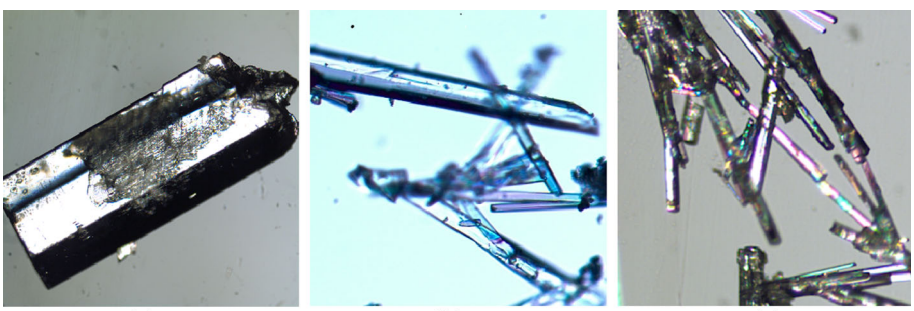

(a) **(b)** **(c)**

Fig. 1 Single crystals of adducts **1** (**a**), **2** (**b**), and **4** (**c**)

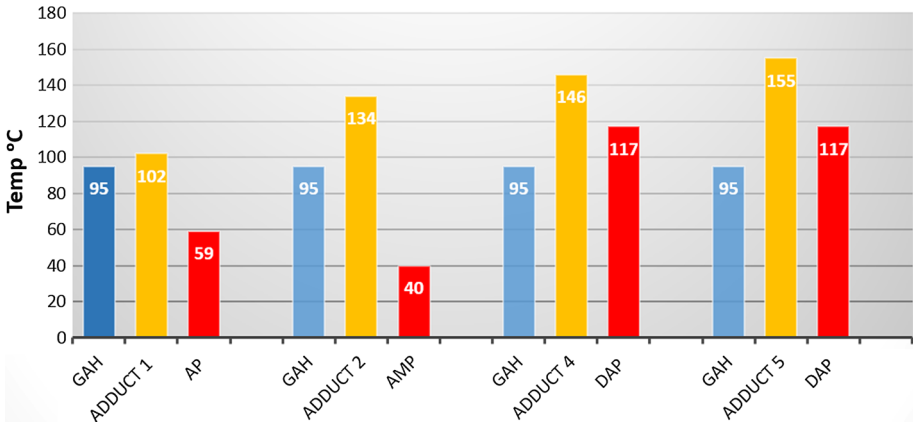

Fig. 2 Comparison of melting points for starting materials and final salts **1, 2, 4,** and **5** obtained from ethanol solution

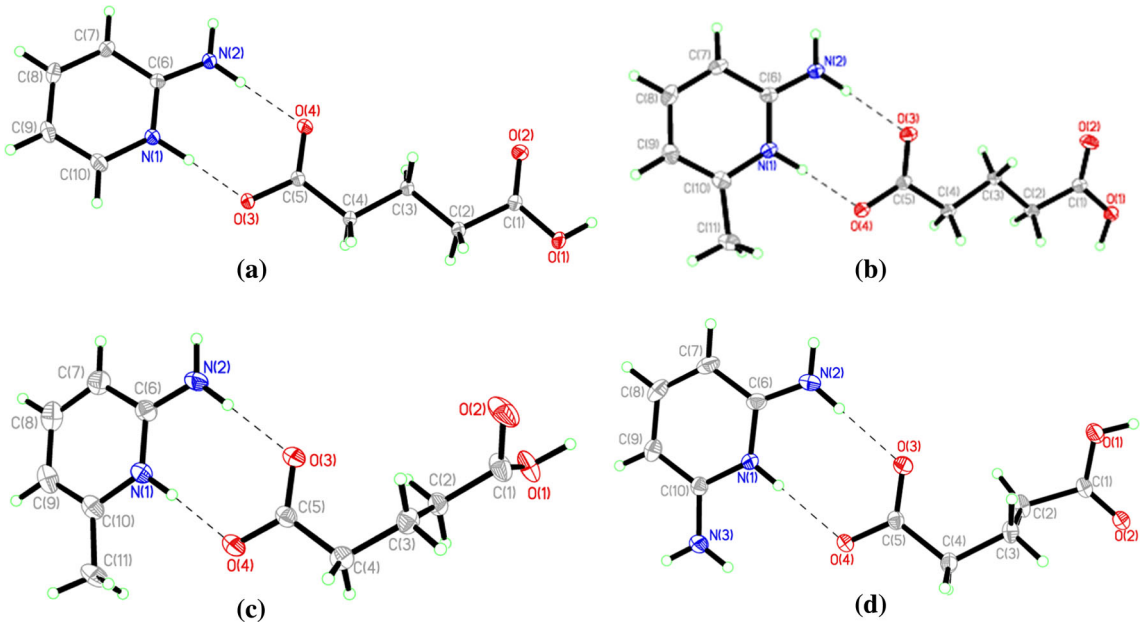

Fig. 3 ORTEP drawings for **1** (**a**), **2** (**b**), **3** (**c**), and **4** (**d**) with labeling scheme and hydrogen bonds between the species shown by *dotted lines*

head-to-tail chain. This type of head-to-tail association of hydrogen glutarate anions has also been observed in the structures of pyrimethamine hydrogen glutarate [39], itraconazole hydrogen glutarate [23], and 2,6-diamino-4-chloropyrimidinium hydrogen glutarate [59]. In common, the layer in **1** is sustained by five unique hydrogen bonds, wherein each strong H-donor (OH, NH-group) acts as a single donor, while both carboxylate oxygen atoms act as double acceptors. All strong H-bonds are gathered within the layer, the layers are situated parallel to the (102) plane, and the only contact C(4)···O(2)($x + 1$, y, z) = 3.4483(15) Å connects parallel layers (Fig. 4b; Table 2). Unexpectedly, structure **1** shows similarities to the 2,6-diamino-4-chloropyrimidinium hydrogen glutarate [59] indicating that the crystal packing may remain intact to the extra substituents in the base molecule such as chlorine atom and the next amino group.

Compounds **2–4** that are the next members in the pool of 1:1 adducts crystallize in the same non-centrosymmetric orthorhombic $P2_12_12_1$ space group and include a pair of polymorphs, compounds **2** and **3**, and compound **4** that is isoelectronic to both of them and isomorphous to compound **3**, since they differ slightly by the unit cell parameters c, unit cell volumes, and crystal densities (Table 1) due to the replacement of the methyl group in **2** and **3** by the amino group in **4**. The very like shapes of these crystals (Fig. 1b, c) might serve as a preliminary indication to the possible similarities in their internal structures [60]. The comparison of the overlay diagrams in pairs **2** and **3** (Fig. 5a), **3** and **4** (Fig. 5b), as well as the overlay of four

Table 2 Selected hydrogen bonds in compounds **1–6**

D–H···A	d(D–H) (Å)	d(H···A) (Å)	d(D···A) (Å)	∠(DHA) (°)	Symmetry operation for acceptor
1					
O(1)–H(1O1)···O(3)	0.91(2)	1.68(2)	2.5643(12)	165(2)	$x - 1, 3/2 - y, z + 1/2$
N(1)–H(1N)···O(3)	1.00(2)	1.68(2)	2.6797(13)	177(2)	x, y, z
N(2)–H(2N)···O(4)	0.90(2)	1.89(2)	2.7860(14)	177(2)	x, y, z
N(2)–H(3N)···O(4)	0.92(2)	1.97(2)	2.7994(14)	149(2)	$1 - x, 2 - y, 2 - z$
C(7)–H(7)···O(2)	0.93	2.44	3.2234(15)	142	$1 - x, 2 - y, 2 - z$
C(4)–H(4A)···O(2)	0.97	2.57	3.4483(15)	151	$x + 1, y, z$
2					
O(1)–H(1O1)···O(4)	0.97(3)	1.62(3)	2.5853(17)	173(3)	$1 - x, y - 1/2, 1/2 - z$
N(1)–H(1N)···O(4)	0.95(2)	1.86(2)	2.8068(19)	174(2)	$x + 1, y - 1, z$
N(2)–H(2N)···O(3)	0.89(2)	1.91(2)	2.801(2)	178(2)	$x + 1, y - 1, z$
N(2)–H(3N)···O(3)	0.93(2)	1.98(2)	2.8187(19)	150(2)	$x + 1/2, 1/2 - y, -z$
C(4)–H(4B)···O(1)	0.99	2.51	3.422(2)	153.6	$2 - x, y + 1/2, 1/2 - z$
C(7)–H(7)···O(2)	0.95	2.47	3.237(2)	138.1	$x - 1/2, 1/2 - y, -z$
3					
O(1)–H(1O1)···O(4)	0.89(4)	1.73(4)	2.602(2)	163(4)	$-x, y - 1/2, 3/2 - z$
N(1)–H(1N)···O(4)	0.92(3)	1.81(3)	2.729(3)	174(3)	$x + 1, y, z$
N(2)–H(2N)···O(3)	0.95(3)	1.86(3)	2.798(3)	172(3)	$x + 1, y, z$
N(2)–H(3N)···O(3)	0.92(3)	1.93(3)	2.823(2)	163(2)	$x + 1/2, 1/2 - y, 1 - z$
C(7)–H(7)···O(2A)	0.93	2.52	3.071(4)	118	$x - 1/2, 1/2 - y, 1 - z$
C(7)–H(7)···O(2)	0.93	2.53	3.229(5)	132	$x - 1/2, 1/2 - y, 1 - z$
C(11)–H(11C)···(1)	0.96	2.46	3.342(3)	152	$-x, y + 1/2, 3/2 - z$
4					
O(1)–H(1O1)···O(4)	0.93(3)	1.62(3)	2.5510(15)	174(3)	$1/2 - x, 1 - y, z + 1/2$
N(1)–H(1N)···O(4)	0.85(2)	2.00(2)	2.8453(15)	172(2)	$-x, y + 1/2, 1/2 - z$
N(2)–H(2N)···O(3)	0.87(2)	1.91(2)	2.7810(19)	174(2)	$-x, y + 1/2, 1/2 - z$
N(2)–H(3N)···O(3)	0.88(3)	1.96(3)	2.8340(17)	169(2)	$1/2 - x, 1 - y, z - 1/2$
N(3)–H(4N)···O(2)	0.90(2)	2.03(2)	2.7973(18)	143(2)	$x - 1/2, 3/2 - y, 1 - z$
N(3)–H(5N)···O(2)	0.83(3)	2.19(3)	2.9859(18)	159(2)	x, y, z
5					
N(1)–H(1N)···O(3)	0.95(2)	1.71(2)	2.6522(17)	170(2)	$2 - x, y + 1/2, 1/2 - z$
N(2)–H(2N)···O(4)	0.91(2)	1.96(2)	2.862(2)	176(2)	$2 - x, y + 1/2, 1/2 - z$
N(2)–H(3N)···O(4)	0.89(2)	1.95(2)	2.8171(18)	165(2)	x, y, z
N(3)–H(4N)···O(3)	0.88(2)	2.50(2)	3.187(2)	135(2)	$2 - x, y + 1/2, 1/2 - z$
N(3)–H(5N)···O(1)	0.94(2)	1.89(2)	2.7939(18)	161(2)	$1 - x, y - 1/2, 1/2 - z$
N(4)–H(6N)···O(1)	0.99(2)	1.69(2)	2.6737(17)	172(2)	$1 - x, 1 - y, -z$
N(5)–H(7N)···N(3)	0.88(2)	2.58(2)	3.416(2)	158(2)	$x, 1/2 - y, z - 1/2$
N(5)–H(8N)···O(2)	0.87(2)	2.01(2)	2.881(2)	177(2)	$2 - x, 1 - y, -z$
N(6)–H(9N)···O(2)	0.89(2)	1.96(2)	2.8487(19)	175(2)	$1 - x, 1 - y, -z$
N(6)–H(10N)···O(3)	0.87(2)	2.16(2)	2.967(2)	154(2)	$x - 1, y, z$
6					
N(2)–H(2N)···O(2)	0.85(2)	2.32(2)	3.156(3)	170(3)	$1/2 - x, y + 1/2, 3/2 - z$
N(3)–H(3N)···O(3)	0.88(2)	2.16(2)	2.983(3)	154(3)	$x, y + 1, z$
N(3)–H(4N)···O(1)	0.88(2)	2.29(2)	3.154(3)	167(3)	$x, y + 1, z$
N(4)–H(5N)···O(1)	0.89(2)	1.81(2)	2.692(3)	174(3)	$x, y + 1, z$
N(5)–H(6N)···O(2)	0.85(2)	2.11(2)	2.951(3)	172(3)	x, y, z
N(6)–H(8N)···O(2)	0.85(2)	1.99(2)	2.834(3)	172(3)	$x, y + 1, z$
N(6)–H(9N)···N(1)	0.86(2)	2.11(2)	2.961(3)	174(3)	$x, 2 - y, z - 1/2$

Table 2 continued

D–H···A	d(D–H) (Å)	d(H···A) (Å)	d(D···A) (Å)	∠(DHA) (°)	Symmetry operation for acceptor
N(7)–H(10 N)···O(3)	0.90(2)	1.87(2)	2.766(3)	177(3)	$x, y + 1, z$
N(8)–H(11N)···N(3)	0.86(2)	2.37(2)	3.204(3)	163(3)	x, y, z
N(8)–H(12N)···O(4)	0.85(2)	2.06(2)	2.898(3)	168(3)	x, y, z
N(9)–H(14N)···O(1S)	0.85(2)	2.12(2)	2.969(3)	175(3)	$-x, y + 1, 3/2 - z$
N(9)–H(13N)···O(4)	0.87(2)	1.99(2)	2.858(3)	175(3)	$x, y + 1, z$

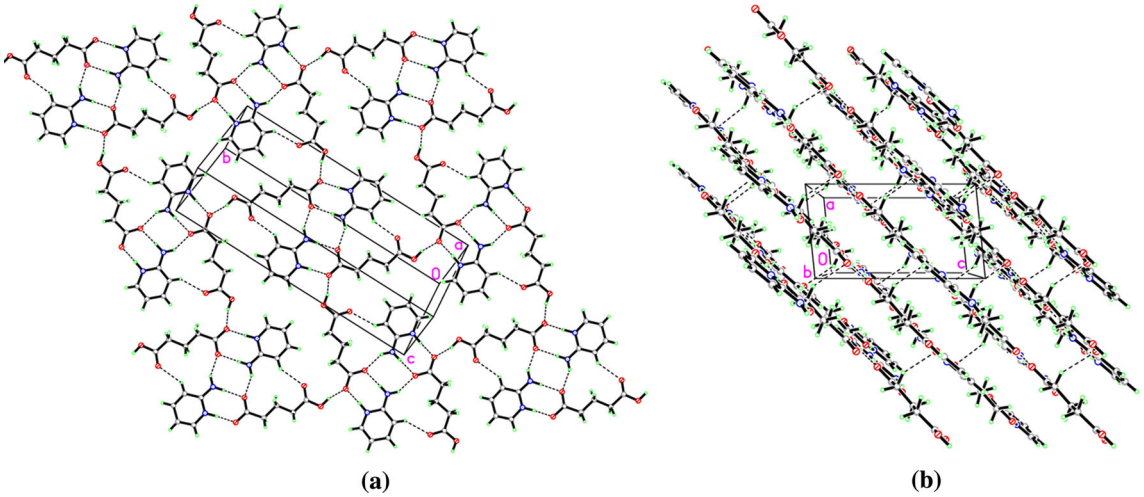

Fig. 4 Fragments of crystal packing in **1**: (**a**) the H-bonded layer; (**b**) packing of the layers

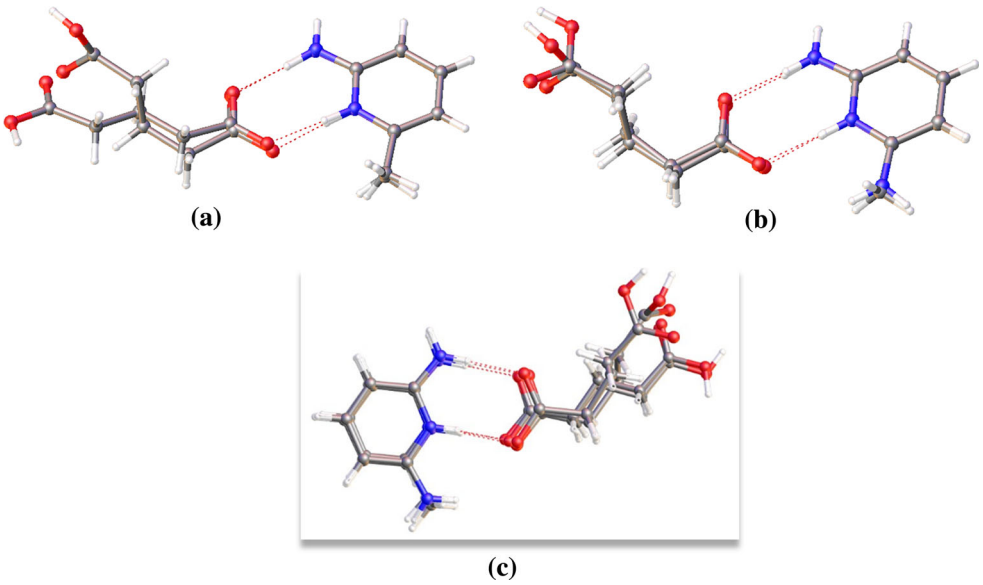

Fig. 5 Overlay diagrams for **2** and **3** (**a**); **3** and **4** (**b**); **1–4** (**c**)

adducts (Fig. 5c), depicted in Fig. 5 reveals the perfect fit of the base molecules in both pairs, the slight twist in the $R_2^2(8)$ heteromeric H-bonded synthons, and significant change in the conformation of hydrogen glutarate residue accompanied even by the rotation of OH- hydrogen atom along the C–O bond as it is seen in structure **2** (Fig. 5a).

The crystallization of all three compounds in the non-centrosymmetric $P2_12_12_1$ space group signifies an

importance of helical patterns produced in the crystals due to the favorable *ortho*-arrangement of NH_2-group to the pyridine nitrogen. It results in interconnection of two helical motifs. The first one in all three crystals is generated by the 2_1 axis along the shortest crystallographic *a* axis and combines the adjacent binary adducts via the second H-atom of N(1)-amino group (Fig. 6a,c), while the second one, being the homomeric self-association of the hydrogen glutarate anions through the above-mentioned $COOH\cdots COO^-$ homosynthon with C(8) graph notation, is generated by the 2_1 axis parallel to the crystallographic *b* direction in **2** and *c* direction in **3** (Fig. 6b,d). The interconnection of these two helical motifs in the H-bonded 3D networks occurs via CH_3 or NH_2-substituents in the second *ortho*-position to the pyridinium nitrogen atoms, sustained by the CH···O interactions in **2** and **3**, and NH···O interactions in **4** (Table 2). Likewise, an inspection of CSD reveals at least three more relative structures, 2-amino-5-bromopyridinium hydrogen glutarate (refcode DUSQAK [56]), 2-amino-5-chloropyridinium hydrogen glutarate (refcode DUSIYA [57]), and 2-amino-5-methylpyridinium 4-carboxybutanoate (refcode YUQKOL [61]) that crystallize in the similar manner in the same $P2_12_12_1$ space group with the close unit cell dimensions. In fact, the space group $P2_12_12_1$ of these crystals also reflects the possibility to consider these materials to manifest the second-harmonic generation (SHG).

Adducts $(HDAP)_2(GA)$ (5) and $(HDAP)_2(DAP)(GA)(EtOH)$ (6) with the 1:2 and 1:3 acid:base molar ratios

The co-crystallization of DAP with GAH_2 from ethanol (EtOH) resulted in adducts **5** and **6** enriched by the basic component. Compound **5** crystallizes in the monoclinic centrosymmetric $P2_1/c$ space group. The asymmetric unit comprises two monoprotonated HDAP cations, and one fully deprotonated glutarate dianion GA, all three species occupying general positions. The content of the asymmetric unit with the principal hydrogen bonds between the components is shown in Fig. 7a. The molecular geometry of the components corresponds to the reported analogues, and the principal bond distances and angles are listed in Table 1S. The *gauche,trans*-conformation of the GA dianion is accompanied by the angular shape of the molecule with the dihedral angle between the carboxylate groups of 77.9(2)°. Following the proton transfer pathway from the two carboxylic groups of GAH_2 molecule to the

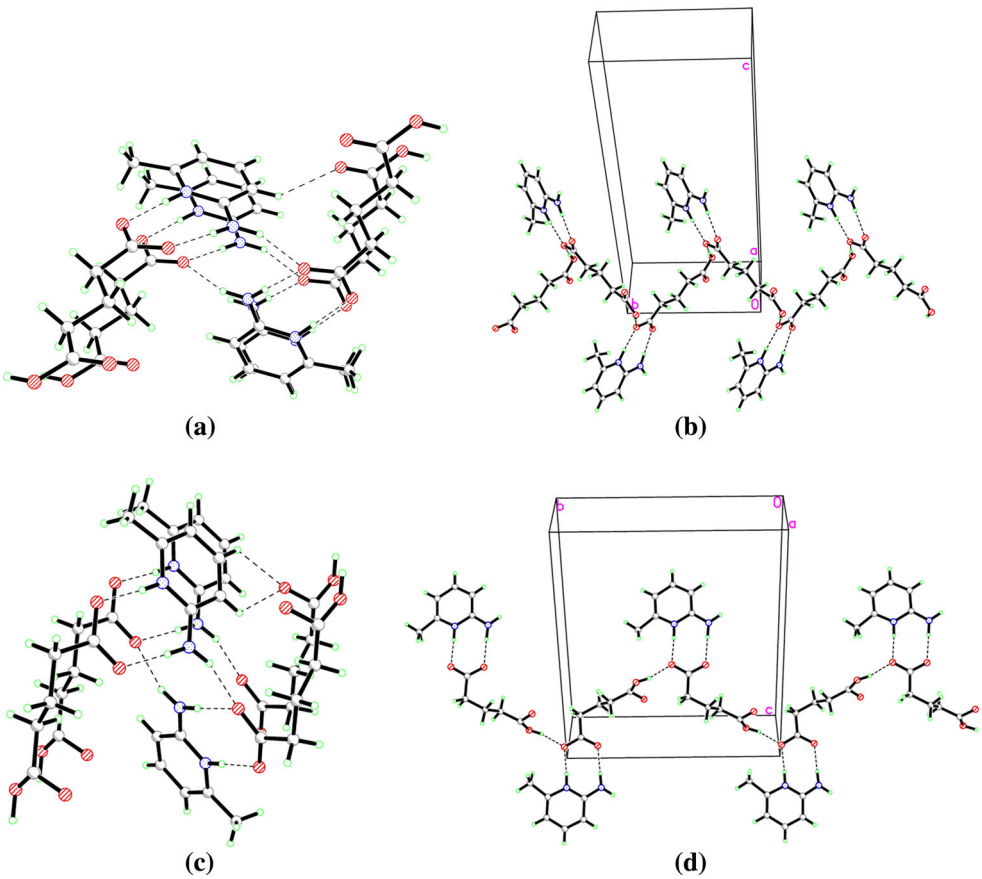

Fig. 6 Virtually similar helical motifs in **2** and **3**. Helices along the crystallographic *a* (**a**) and *b* axes (**b**) in **2**. Helices along the crystallographic *a* (**c**) and *c* axes (**d**) in **3**

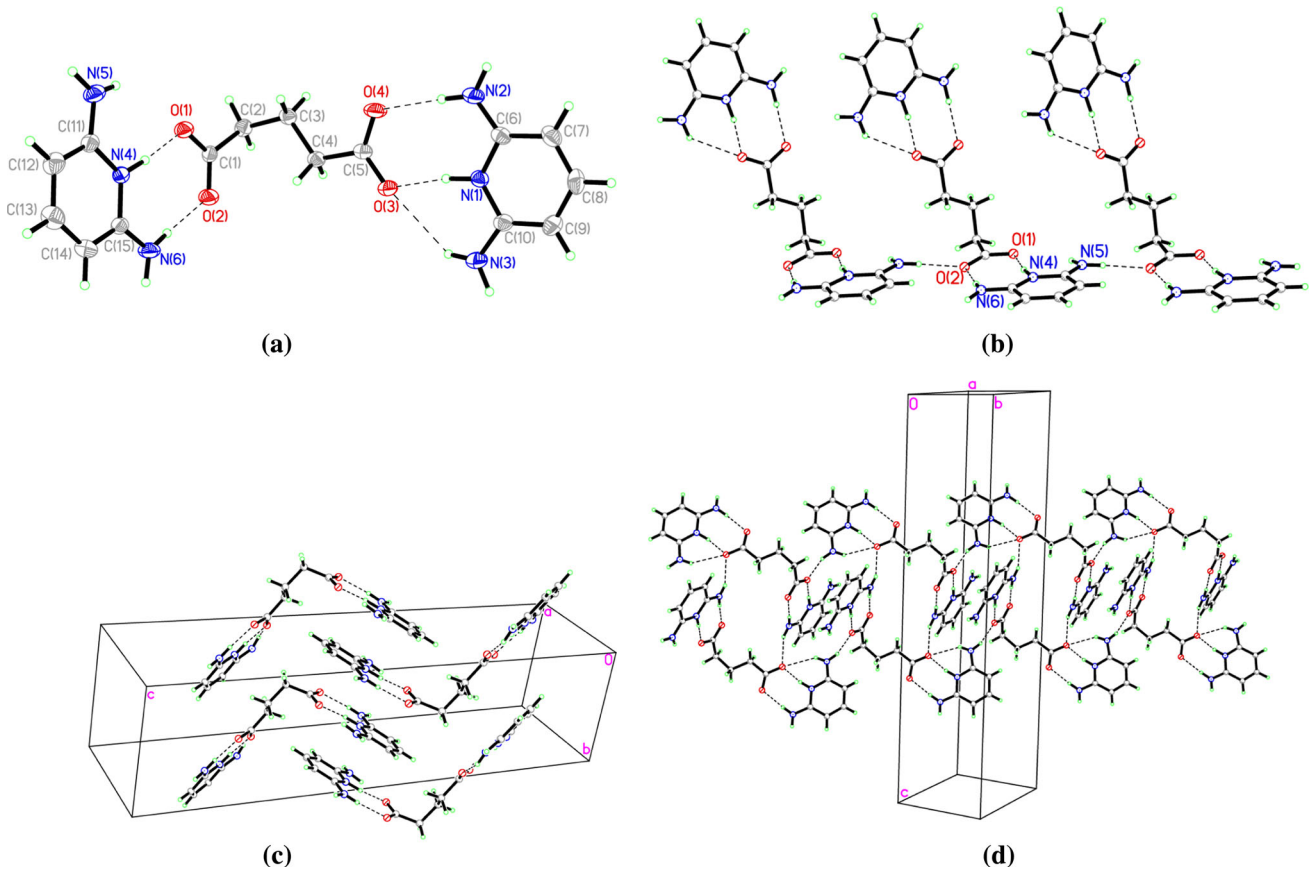

Fig. 7 Structure **5**. (**a**) Content of the asymmetric unit; (**b**) fragment of the H-bonded ribbon; (**c**) stacking of the trimeric units along the crystallographic b axis; (**d**) fragment of 3D crystal packing through interconnection via NH···O hydrogen bonds between trimeric formula units

pyridine moieties of two DAP molecules, the latter ones are attached to the dianion in the asymmetric modes, via two virtually similar $R_2^2(8)$ 2-amino-pyridinium–carboxylate heterosynthons, N···O distances being in the range 2.6522(17)–2.8487(19) Å (Table 2), fused from one side with the $R_2^1(6)$ heterosynthon supported by the single N(3)-H···O(3) hydrogen bond, N···O = 3.187(2) Å. These angular trimeric formula units related by the inversion centers form elegant ribbons along the crystallographic *b* axis through the sequence of alternating H-bonded rings, $R_4^8(20)R_2^2(8)R_8^6(20)$, and hydrogen atoms of amino groups not involved into acid–base interactions within the trimeric unit (Fig. 7b).

In general, the 3D H-bonded network is sustained by ten unique hydrogen bonds that include nine NH···O hydrogen bonds, N···O distances being in the range 2.6522(17)–3.187(2) Å, and one NH···N hydrogen bond, N(5)···N(3) = 3.416(2) Å. An excess of strong H^- donors in the form of amino groups explains the participation of two deprotonated carboxylic oxygen atoms in these interactions as double [O(1), O(2), and O(4)] and even triple [O(3)] H^- acceptors (Table 2).

Compound **6** crystallizes in the monoclinic centrosymmetric *C*2/*c* space group. The asymmetric unit comprises two monoprotonated HDAP cations, one neutral DAP molecule, one fully deprotonated glutarate anion GA, and one molecule of ethanol as a solvent, all species occupying general positions. The content of the asymmetric unit with the principal hydrogen bonds between the components is shown in Fig. 8a. To the best our knowledge, no adducts with such an unusual 1:3 acid:base ratio were reported for GAH_2 so far. The molecular geometry of the components corresponds to the reported analogues, and the principal bond distances and angles are listed in Table 1S. The *trans,gauche*-conformation of the GA dianion is characterized by the near antiparallel arrangement of carboxylate groups with the dihedral angle of 11.8(7)° between the COO^- residues. This resulted in location of two HDAP cations in almost parallel planes as the dihedral angle of 4.7(2)° between their average planes indicates. The neutral DAP and ethanol molecules upraise nearly perpendicular to the charged species, the dihedral angles HDAP(1,2)/DAP are equal to 83.49(7) and 85.05(7)°, while the dihedral angles HDAP(1,2)/EtOH are equal to 80.6(3) and 77.7(3)°.

Following the proton transfer pathway from the two carboxylic groups of GAH_2 molecule to the pyridine moieties of two DAP molecules, these species form the

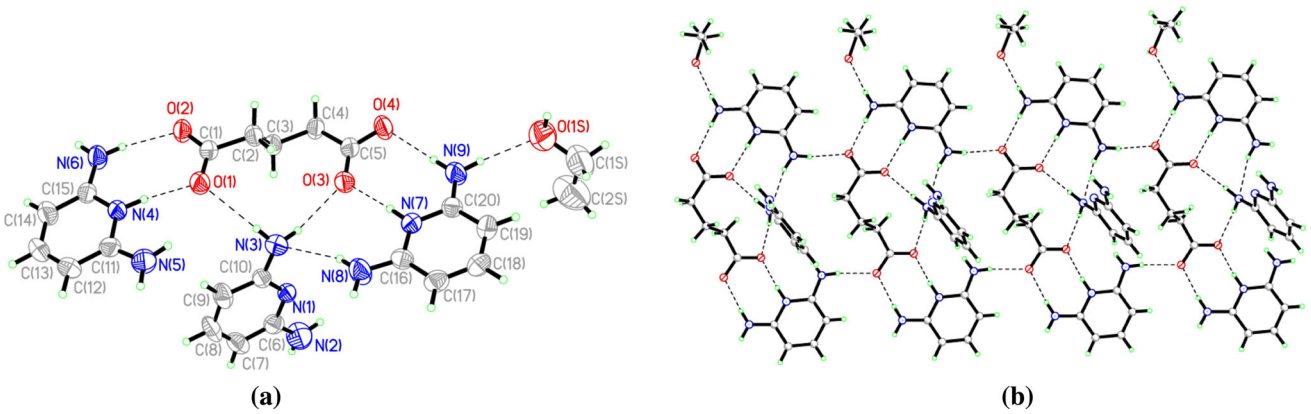

Fig. 8 Structure **6**. (**a**) Content of the asymmetric unit; (**b**) fragment of the H-bonded ribbon

two-level trimeric unit typical for 2-aminopyridine and its analogues in combination with the even-membered aliphatic dicarboxylic acids [19], and sustained by two virtually similar $R_2^2(8)$ 2-aminopyridinium–carboxylate heterosynthons, N···O distances being in the range 2.692(3)–2.858(3) Å. (Table 2). The tri-membered entities related by translation are combined into ribbon via next *o*-NH_2-group from each of pyridinium cations. The neutral DAP molecule situated in the perpendicular plane is anchored to this ribbon in a DDA mode (as a double donor and a single acceptor) suggesting both H-atoms and the lone pair of N(3) nitrogen atom for these interactions, and thus supporting the folded conformation of the GA dianion. In general, the infinite ribbon motif is sustained by nine unique hydrogen bonds, including eight NH···O and one NH···N hydrogen bonds, each NH-group acts as a single donor, and each carboxylic oxygen acts as a double acceptor (Fig. 8b). The combination of these ribbons into 3D H-bonded network in perpendicular direction occurs via neutral DAP and EtOH molecules which both act as H-donors (NH_2- and OH-groups) and H-acceptors (lone pairs of hydroxyl oxygen and pyridine nitrogen atoms).

Finally, the literature overview reveals that the 1:1 acid–base molar ratio is the most commonly met in the co-crystals and salts of glutaric acid. The 1:2 molar ratio is also reported [14, 28, 62, 63], and very few examples such as bis(2-aminopyrimidin-1-ium) bis(glutaric acid) glutarate, *tris*(2-methylimidazolium) hemikis(2-methylimidazole) hydrogen glutarate dihydrate, bis(4-bromobenzamide) bis(glutaric acid) 1,4-dinitrobenzene [43, 64, 65], and the adduct **6** demonstrate quite unusual compositions. The polymorphism that is always an option for multicomponent solids [66, 67] has been registered in the glutaric acid–glycine, and glutaric acid–2-aminopyrimidine multicomponent series [42, 43].

Alongside the others [40, 43], herein we registered the conformation flexibility of glutaric acid in its neutral, mono- and di-deprotonated ionic forms. The literature data together with the examples reported herein show that glutaric acid in adducts can be found in both *trans,trans*-conformations as in **1** and **2**, and in *trans,gauche*-conformations as in **3–6**. In order to understand why co-crystallization can easily change its conformation, the energy difference between the two conformers was evaluated using quantum chemical calculations (Gaussian 09, B3LYP/6-311G* with optimized molecular geometry) [68]. Insignificant difference (0.19 kcal/mol) in total energy was found between the two conformations. Considering that rotational barrier around the C–C bonds is low, it is possible to suggest that molecular conformation of glutaric acid in the crystal is mostly defined by its packing and hydrogen-bonding patterns.

Conclusions

A new series of glutaric acid adducts with a range of 2-aminopyridine derivatives, 2-aminopyridine, 2-amino-6-methylpyridine, and 2,6-diaminopyridine were synthesized using solvent-assisted evaporation-based crystallization. Four crystalline adducts obtained from methanol have 1:1 acid:base molar ratio. In the case of crystallization from ethanol with the higher 2,6-diaminopyridine base content, two more multicomponent solids with the 1:2 and 1:3 acid:base molar ratios were also obtained. In all cases, the formation of supramolecular complexes is affected by the geometrical compatibility between the 2-aminopyridine base and glutaric acid, and by the N–H···O hydrogen bonds with a graph of $R_2^2(8)$. The self-association of hydrogen glutarate monoanion into corrugated chain in the 1:1 adducts is governed by strong COOH···COO^- hydrogen

bond. The extra number of strong H-donors in the form of amino groups was equalized by the functions of carboxylic groups as double and even triple acceptors, and in the case 2,6-DAP) by the base self-assembling, thus excluding the water inclusion to overcome this misbalance. This work also demonstrates possibilities of chemical (neutral, mono-, di-anion) and conformational diversity of glutaric acid in the H-bonded adducts. Within investigated supramolecular complexes, three of them crystallize in an acentric space group $P2_12_12_1$ (**2–4**) can represent intriguing objects for further investigation of their NLO properties.

Supplementary data

CCDC 1418224-1418226, CCDC 1460852-1460853, and CCDC 1472465 contain the supplementary crystallographic data for **1–6**. These data can be obtained free of charge via www.ccdc.cam.ac.uk/data_request/cif, or by emailing data_request@ccdc.cam.ac.uk, or by contacting The Cambridge Crystallographic Data Centre, 12, Union Road, Cambridge CB2 1EZ, UK; fax: +44 1223 336033. The Supporting Information includes Table containing selected geometrical parameters for all adducts, IR spectra, and experimental and simulated X-ray diffraction patterns (PDF).

Acknowledgments The authors are grateful for NSF support via DMR-0934212 and DMR-1523611 (PREM), and IIA-1301346.

References

1. Shan N, Zaworotko MJ (2008) Drug Discov Today 13:440–446
2. Remenar JF, Morissette SL, Peterson ML, Moulton B, MacPhee JM, Guzmán HR, Almarsson Ö (2003) J Am Chem Soc 125:8456–8457
3. McNamara DP, Childs SL, Giordano J, Iarriccio A, Cassidy J, Shet MS, Mannion R, O'Donnell E, Park A (2006) Pharm Res 23:1888–1897
4. Childs SL, Chyall LJ, Dunlap JT, Smolenskaya VN, Stahly BC, Stahly GP (2004) J Am Chem Soc 126:13335–13342
5. Qiao N, Li M, Schlindwein W, Malek N, Davies A, Trappitt G (2011) Int J Pharm 419:1–11
6. Sekhon BS (2009) Ars Pharm 50:99–117
7. Surov AO, Manin AN, Voronin AP, Drozd KV, Simagina AA, Churakov AV, Perlovich GL (2015) Eur J Pharm Sci 77:112–121
8. Curiel D, Mas-Montoya M, Sanchez G (2015) Coord Chem Rev 284:19–66
9. Fighera MR, Royes LFF, Furian AF, Schneider Oliveira M, Fiorenza NG, Frussa-Filho R, Petry JC, Coelho RC (2006) Neurobiol Dis 22:611–623
10. Geib SJ, Vincent C, Fan E, Hamilton AD (1993) Angew Chem Int Ed 32:119–121
11. Karle IL, Ranganathan D, Haridas V (1997) J Am Chem Soc 119:2777–2783
12. Goswami S, Ghosh K, Dasgupta S (2000) J Org Chem 65:1907–1914
13. Aakeröy CB, Hussain I, Desper J (2006) Cryst Growth Des 6:474–480
14. Vishweshwar P, Nangia A, Lynch VM (2003) Cryst Growth Des 3:783–790
15. Aakeröy CB, Rajbanshi A, Li ZJ, Desper J (2010) CrystEngComm 12:4231–4239
16. Mukherjee A, Desiraju GR (2014) Cryst Growth Des 14:1375–1385
17. Bhattacharya S, Saraswatula VG, Saha BK (2013) Cryst Growth Des 13:3651–3656
18. Braga D, Dichiarante E, Palladino G, Grepioni F, Chierotti MR, Gobetto R, Pellegrino L (2010) CrystEngComm 12:3534–3536
19. Sandhu B, Fonari MS, Sawyer K, Timofeeva TV (2013) J Mol Struct 1052:125–134
20. Videnova-Adrabinska V, Etter MC (1995) J Chem Crystallogr 25:823–829
21. Aakeröy CB, Panikkattu SV, DeHaven B, Desper J (2012) Cryst Growth Des 12:2579–2587
22. Gopalan RS, Kumaradhas P, Kulkarni GU, Rao CNR (2000) J Mol Struct 521:97–106
23. Shevchenko A, Miroshnyk I, Pietila LO, Haarala J, Salmia J, Sinervo K, Mirza S, van Veen B, Kolehmainen E, Nonappa YJ (2013) Cryst Growth Des 13:4877–4884
24. Cheney ML, Weyna DR, Shan N, Hanna M, Wojtas L, Zaworotko MJ (2010) Cryst Growth Des 10:4401–4413
25. Trask AV, Motherwell WDS, Jones W (2004) Chem Commun 890–891
26. Lemmerer A, Bernstein J, Kahlenberg V (2010) CrystEngComm 12:2856–2864
27. Caira MR, Bourne SA, Samsodien H, Engel E, Liebenberg W, Stieger N, Aucamp M (2012) CrystEngComm 14:2541–2551
28. Hu Y, Gniado K, Erxleben A, McArdle P (2014) Cryst Growth Des 14:803–813
29. Childs SL, Wood PA, Rodriguez-Hornedo N, Reddy LS, Hardcastle KI (2009) Cryst Growth Des 9:1869–1888
30. Karki S, Friscic T, Jones W (2009) CrystEngComm 11:470–481
31. Yan Y, Chen JM, Lu TB (2013) CrystEngComm 15:6457–6460
32. Espinosa-Lara JC, Guzman-Villanueva D, Arenas-Garcia JI, Herrera-Ruiz D, Rivera-Islas J, Roman-Bravo P, Morales-Rojas H, Höpfl H (2013) Cryst Growth Des 13:169–185
33. Félix-Sonda BC, Rivera-Islas J, Herrera-Ruiz D, Morales-Rojas H, Höpfl H (2014) Cryst Growth Des 14:1086–1102
34. Kastelic J, Hodnik Z, Sket P, Plavec J, Lah N, Leban I, Pajk M, Planinsek O, Kikelj D (2010) Cryst Growth Des 10:4943–4953
35. Trask AV, Motherwell WDS, Jones W (2006) Int J Pharm 320:114–123
36. Robert JJ, Raj SB, Muthiah PT (2001) Acta Crystallog E57:o1206–o1208
37. Chadha R, Saini A, Khullar S, Jain DS, Mandal SK, Guru Row TN (2013) Cryst Growth Des 13:858–870
38. Sládková V, Cibulková J, Eigner V, Šturc A, Kratochvíl B, Rohlíček J (2014) Cryst Growth Des 14:2931–2936
39. Stanley N, Sethuraman V, Muthiah PT, Luger P, Weber M (2002) Cryst Growth Des 2:631–635
40. Sanphui P, Tothadi S, Ganguly S, Desiraju GR (2013) Mol. Pharmaceutics 10:4687–4697
41. Inouye S, Iitaka Y (1963) Bull Chem Soc Jap 36:1163–1168
42. Zakharov BA, Losev EA, Kolesov BA, Drebushchak VA, Boldyreva EV (2012) Acta Crystallogr B 68:287–296
43. Odiase I, Nicholson CE, Ahmad R, Cooper J, Yufit DS, Cooper SJ (2015) Acta Crystallogr C 71:276–283
44. Jin S, Zhao Y, Liu B, Jin X, Zhang H, Wen X, Liu H, Jin L, Wang D (2015) J Mol Struct 1099:601–615

45. SAINT+, Version 6.45, Bruker AXS Inc., Madison, Wisconsin, USA, 2003
46. Sheldrick GM (1997) SADABS, Program for Empirical Absorption Correction of Area Detector Data, University of Gottingen, Germany
47. Sheldrick GM (2015) Acta Crystallogr C 71:3–8
48. Etter MC (1991) J Phys Chem 95:4601–4610
49. Etter MC (1990) Acc Chem Res 23:120–126
50. Etter MC, MacDonald JC, Bernstein J (1990) Acta Crystallogr B 46:256–262
51. Bernstein J, Davis RE, Shimoni L, Chang NL (1995) Angew Chem Int Ed Eng 34:1555–1573
52. Thapa S, Draguta S, Sandhu B, Antipin MY, Timofeeva TV (2013) Acta Crystallogr E69:o670
53. Chao M, Schemp E, Rosenstein RD (1975) Acta Crystallogr B 31:2922–2924
54. Draguta S, Khrustalev VN, Sandhu B, Antipin MY, Timofeeva TV (2012) Acta Crystallogr E68:o3466
55. Callear SK, Hursthouse MB, Threlfall TL (2010) CrystEngComm 12:898–908
56. Hemamalini M, Fun HK (2010) Acta Crystallogr E66:o1964
57. Hemamalini M, Fun HK (2010) Acta Crystallogr E66:o2008–o2009
58. Aakeroy CB, Hussain I, Forbes S, Desper J (2007) CrystEngComm 9:46–54
59. Edison B, Balasubramani K, Thanigaimani K, Khalib NC, Arshad S, Razak IA (2014) Acta Crystallogr E70:o857–o858
60. Yakovenko AA, Gallegos JH, Antipin MY, Masunov A, Timofeeva TV (2011) Cryst Growth Des 11:3964–3978
61. Hemamalini M, Fun HK (2010) Acta Crystallogr E66:o1841–o1842
62. Chan HCS, Woollam GR, Wagner T, Schmidt MU, Lewis RA (2014) CrystEngComm 16:4365–4368
63. Hutchins KM, Sumrak JC, Swenson DC, MacGillivray LR (2014) CrystEngComm 16:5762–5764
64. Lawniczak P, Pogorzelec-Glaser K, Pawlaczyk C, Pietraszko A, Sczeniak L (2009) J Phys Condens Matter 21:345403 (9 pp)
65. Tothadi S, Sanphui P, Desiraju GR (2014) Cryst Growth Des 14:5293–5302
66. Aitipamula S, Chow PS, Tan RBH (2014) CrystEngComm 16:3451–3465
67. Tothadi S (2014) CrystEngComm 16:7587–7597
68. Frisch MJ et al. (20090 Gaussian 09, revision D.01; Gaussian, Inc.: Wallingford, CT